# High-frequency dynamical response of Abrikosov vortex lattice in flux-flow region

F. Pei-Jen Lin*
*NCTS, National Tsing Hua University, Hsinchu 300, Taiwan*

Peter Matlock†
*Research Department, Universal Analytics Inc., Airdrie, Alberta, T4B 2A4 Canada*

(Received 6 March 2010; revised manuscript received 25 June 2010; published 22 July 2010)

The dynamical response of the Abrikosov vortex lattice in the presence of an oscillating driving field is calculated by constructing an analytical solution of the time-dependent Ginzburg-Landau equation. The solution is steady state, and work done by the input signal is dissipated through vortex cores, mainly by scattering with phonons. The solution shows nonlinear response; the existence of well-defined parameters to control nonlinear effects is important for any practical application in electronics and a normalized distance from the normal-superconducting phase-transition boundary is found to be such a parameter to which the response is sensitive. Favorable comparison with NbN experimental data in the optical region is made, where the effect is in the linear regime. Predictions are put forward regarding the suppression of heating and also the lattice configuration at high frequency.

DOI: 10.1103/PhysRevB.82.024516 PACS number(s): 74.20.De, 74.25.N−, 74.40.Gh, 74.25.Ha

## I. INTRODUCTION

Superconducting films are candidate substances for the improvement of electronics technology in a myriad of applications. While the low resistance is very attractive in this regard, it has proved difficult to control the nonlinear behavior of such materials in response to electromagnetic field.[1] When a magnetic field is strong enough to penetrate into a superconductor, it does so in the form of quantized magnetic flux tubes. The resulting vortex matter is a mixed state with both superconducting phase and normal-phase vortex cores. Vortices are surrounded by a supercurrent and can be forced into motion by the current resulting from an applied electric field.

As a topological defect, a vortex is not only stable under perturbations[2,3] but cannot decay. The collection of vortices in a type-II superconductor forms what is called vortex matter, and it is this which determines the physical properties of the system rather then the underlying material properties, in particular, driving phase transitions.[2,4] In the mixed state, a superconductor is not perfect; it exhibits neither perfect diamagnetism nor zero electrical resistance. The transport current $\mathbf{J}$ generates a Lorentz force $\mathbf{F}=\Phi_0\mathbf{J}\times\hat{\mathbf{h}}$ on the vortex and forces it into motion, dissipating energy.

In reaching thermal equilibrium, energy is transferred via interactions between phonons and quasiparticle excitations. Small-scale imperfections such as defects scatter the quasiparticles, affecting their dynamics. In *dirty* superconductors, impurities are plentiful and vortices experience a large friction. This implies a fast momentum-relaxation process. In contrast is the *clean* limit, where impurities are rare and no such relaxation process is available. It is in this situation of slow relaxation that the Hall effect appears.

Generally, the *H-T* phase diagram[4] of the vortex matter has two phases. In the *pinned phase* vortices are trapped by an attractive potential due to the presence of large-scale defects, thus resistivity vanishes. This phase contains what are known as glass states. There is then the *unpinned phase* in which vortices can move when forced and so a finite resistivity appears. This phase is also known as the flux-flow region and can be of two types. One type is a liquid state where vortices can move independently; the other type is a solid state in which vortices form a periodic Abrikosov lattice[5] resulting from their long-range interaction. One model for the transition between the pinned and unpinned phases appears in Ref. 6.

In the unpinned phase, the system is driven from equilibrium and experiences a relaxation process. There are several ways to describe such a system. A microscopic description[7] invoking interactions between a vortex and quasiparticle excitations at the vortex core provides a good understanding of friction and sports good agreement with experiments in the sparse-vortex region $H \ll H_{c2}$. There is also a macroscopic description, the London approach, where vortices are treated either as interacting pointlike particles or an elastic manifold subject to a pinning potential, driving force and friction.[8,9] In the small-field region, vortices behave as an array of elastic strings.

In the dense-vortex region $H \gg H_{c1}$, where the magnetic field is nearly homogeneous due to overlap between vortices, Ginzburg-Landau (GL) theory, which describes the system as a field, provides a more reasonable model. In dynamical cases, time-dependent GL (TDGL) theory is appropriate;[7,10,11] in GL-type models, additional simplification can come from the lowest Landau-level (LLL) approximation which has proven to be successful in the vicinity of the superconducting-normal (S-N) phase-transition line $H \sim H_{c2}$. This has been pursued in the static case[4] (without driving force) and in the dynamic case with a time-independent transport current.[12] It may be noted that in the glass state, zero resistance within the LLL approximation cannot be attained.[13]

Based on TDGL theory, we will study the dynamical response of a dense vortex lattice forced into motion by an alternating current induced by an external electromagnetic field. Vortices are considered which are free from being pinned and thermally excited, which in addition to thermal

 

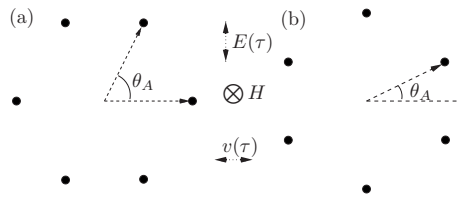


FIG. 1. Possible vortex lattice configurations. (a) Typical large angle, plotted for $\theta_A=60°$; (b) typical small angle, plotted for $\theta_A=30°$. In the static case, $\theta_A=60°$ and $\theta_A=30°$ will correspond to the same energy. The applied magnetic field $\mathbf{H}$ is along the $-z$ direction and electric field $\mathbf{E}(\tau)$ along the $y$ direction. $\theta_A$ is the apex angle of the two defining lattice vectors. The two vectors for the rhombic vortex lattice are $\mathbf{a}_1=(\sqrt{2\pi/\wp},0)$ and $\mathbf{a}_2=(\sqrt{2\pi/\wp}/2,\sqrt{2\pi\wp})$, where $\wp=\frac{1}{2}\tan\theta_A$. The motion of vibrating vortices is indicated by the horizontal arrow.

noise would produce entanglement and bending. We assume the vortices can transfer work done by an external field to a heat bath. Experimentally, a low-temperature superconductor far away from the clean limit is the best candidate for attaining these conditions. We do not consider thermal fluctuation effects specific to high-temperature superconductors. In a dissipative system driven by a single-harmonic electric field $E\cos\Omega\tau$, long after its saturation time we can expect the system to have settled into steady-state behavior, where the vortices are vibrating periodically with some phase.

The TDGL model in the presence of external electromagnetic field is analyzed and solved in Sec. II. The dynamical S-N phase-transition surface $\tilde{T}_c(H,E,\Omega)$ is located in $\{T,H,E,\Omega\}$ space. This surface coincides with the mean-field upper-critical field $H_{c2}(T)$ in the absence of the applied field and with the phase-transition surface in the presence of the constant driving field considered by Hu and Thompson.[10] We will provide an analytical formalism for perturbative expansion in the distance to $\tilde{T}_c$, valid in the flux-flow region. The response of vortex matter forced into motion by the transport current is studied in Sec. III. The current-density distribution and the motion of vortices are treated in Sec. III A. In analyzing the vortex lattice configuration in Sec. III B, a method is utilized whereby the heat-generation rate is maximized. Next are discussed power dissipation, generation of higher harmonics, and the Hall effect. An experimental comparison is made in Sec. IV with far-infrared (FIR) measurement on NbN. Finally, some conclusions are made in Sec. V.

## II. FLUX-FLOW SOLUTION

Let us consider a dense vortex system prepared by exposing a type-II superconducting material to a constant external magnetic field $\mathbf{H}=(0,0,-H)$ with magnitude $H_{c2}>H\gg H_{c1}$. We also select the $c$ axis of the superconductor to be in the $z$ direction. Let the superconductor carry an alternating electric current along the $y$ direction, generated by an electric field $E(\tau)=E\cos\Omega\tau$ as shown in Fig. 1. Such a system when disturbed from its equilibrium state will undergo a relaxation process. For our system, the TDGL equation[10,14] is a useful extension of the equilibrium GL theory.

In the dense-vortex region of the $H$-$T$ phase diagram, vortices overlap and a homogeneous magnetic field obtains. Describing the response of such a system by a field, the order parameter $\Psi$ in the GL approach, is more suitable than describing vortices as particlelike flux tubes, as is done in the London approach.[8]

### A. Time-dependent Ginzburg-Landau model

A strongly type-II superconductor is characterized by its large penetration depth $\lambda$ and small coherence length $\xi$, $\kappa\equiv\lambda/\xi\gg1$. The difference between induced magnetic field and external magnetic field is $\mathbf{H}-\mathbf{B}=-4\pi\mathbf{M}$. In the vicinity of the phase-transition line $H_{c2}(T)$ vortices overlap significantly and $\mathbf{H}\approx\mathbf{B}$ making $\mathbf{M}$ small. In this case, the magnetic field may be treated as homogeneous within the sample. We will have in mind an experimental arrangement using a planar sample very thin compared with its lateral dimensions. Since the characteristic length for inhomogeneity of electric field[10] $\xi_E^2=4\pi\lambda^2\sigma_n/\gamma$ is then typically large compared with sample thickness, this implies that the electric field may also be treated as homogeneous throughout,[10,12] eliminating the need to consider Maxwell's equations explicitly.

In equilibrium, the Gibbs free energy of the system is given by[2]

$$F[\Psi]=\int d\mathbf{r}\left\{\frac{\hbar^2}{2m_{ab}}|\mathbf{D}\Psi|^2+\frac{\hbar^2}{2m_c}|\partial_z\Psi|^2-\alpha(T_c^0-T)|\Psi|^2+\frac{\beta}{2}|\Psi|^4\right\},\tag{1}$$

where $T_c^0$ is the critical temperature at zero field. Covariant derivatives employed here preserve local gauge symmetry and are two dimensional; $D_\tau=\partial_\tau+i\frac{e^*}{\hbar}\phi$ and $\mathbf{D}=\nabla^{(2)}-i\frac{e^*}{\hbar c}\mathbf{A}$.

Governing the dynamics of the field $\Psi$ is the TDGL equation,

$$\frac{\hbar^2\gamma}{2m_{ab}}D_\tau\Psi=-\frac{\delta F}{\delta\Psi^*}.\tag{2}$$

This determines the characteristic relaxation time of the order parameter. Microscopic derivation of TDGL can be found in Refs. 7 and 15 in which the values of $\alpha$, $\beta$, and $\gamma$ are studied. In the macroscopic case, these are viewed simply as parameters of the model. At microscopic scale, disorder is accounted for by $\gamma$, the inverse of the diffusion constant; the relation of $\gamma$ to normal-state conductivity is discussed in Appendix A.

In standard fashion, $\mathbf{E}=-\nabla\phi-\frac{1}{c}\partial_\tau\mathbf{A}$ while $\mathbf{B}=\nabla\times\mathbf{A}$. Our set of equations is completed[2] by including Ampère's law, writing for the total current density,

$$\mathbf{J}_0=\left(\frac{c}{4\pi}\right)\nabla\times\nabla\times\mathbf{A}=\sigma_n\mathbf{E}+\mathcal{J}_0.\tag{3}$$

As we shortly make a rescaling of quantities, we have written 0 subscripts here for clarity. The first term is the normal-state conductivity. The second term can be written using a Maxwell-type equation relating the vector potential with the supercurrent,

$$\mathcal{J}_0 = -i\frac{\hbar e^*}{2m_{ab}}[\Psi^*\mathbf{D}\Psi - \Psi(\mathbf{D}\Psi)^*]. \tag{4}$$

This is a gauge-invariant model; we fix the gauge by considering the explicit vector potential $\mathbf{A}=(By,0,0)$ and $\phi = yE\cos\Omega\tau$, corresponding to an alternating transport current. Each vortex lattice cell has exactly one fluxon. We do not assume the electric field and the motion of vortices are in any particular direction relative to the vortex lattice by way of rendering visible any anisotropy.

For convenience, we define some rescaled quantities. The rescaled temperature and magnetic field are $t=T/T_c^0$ and $b=H/H_{c2}^0$. $H_{c2}^0$ denotes the mean-field upper-critical field, extrapolated from the $T_c^0$ region down to zero temperature.

In the *a-b* plane of the crystal we make use of *magnetic length* $\xi_\ell$. We define $\xi_\ell^2=\xi^2/b$, where $\xi^2=\hbar^2/2m_{ab}\alpha T_c^0$. The scale on the *c* axis is $\xi_c/\sqrt{b}$ with $\xi_c^2=\hbar^2/2m_c\alpha T_c^0$. The coordinate anisotropy in $z$ is absorbed into this choice of normalization, as can be seen in Eq. (6). The order parameter $\Psi$ is scaled by $\sqrt{2b\alpha T_c^0/\beta}$. The time scale is normalized as $\tau_s=\gamma\xi_\ell^2/2$. Therefore, frequency is $\omega=\Omega\tau_s$. Note that $\omega$ is then inversely proportional to $b$. The amplitude of the external electric field is normalized with $E_0=2\hbar/e^*\xi^3\gamma$ so that $e=E/E_0$.

After our rescaling the TDGL equation takes the simple form

$$L\Psi - \frac{1}{2b}(1-t)\Psi + |\Psi|^2\Psi = 0, \tag{5}$$

where the operator $L$ is defined as

$$L = D_\tau - \frac{1}{2}\mathbf{D}^2 - \frac{1}{2}\partial_z^2. \tag{6}$$

With our specified vector potential, covariant derivatives are $D_\tau=\partial_\tau+ivy\cos\omega\tau$, $D_x=\partial_x-iy$, and $D_y=\partial_y$. We define $v=eb^{-3/2}$ for convenience. The TDGL equation is invariant under translation in $z$, thus the dependence of the solution in the $z$ direction can be decoupled. $L$ is not Hermitian,

$$L^\dagger = -D_\tau - \frac{1}{2}\mathbf{D}^2 - \frac{1}{2}\partial_z^2, \tag{7}$$

where the conjugation is with respect to the usual inner product defined below.

We will make extensive use of the eigenfunctions of $L$ and $L^\dagger$ in what follows. The eigenvalue equation

$$L\varphi_{n,k_x} = \varepsilon_n\varphi_{n,k_x} \tag{8}$$

defines the set of eigenfunctions of $L$ appropriate for our analysis; this can be seen in Appendix B. The convention is that $\varepsilon_n=\varepsilon_{n'}$ when and only when $n=n'$. By "following the sign" in front of the $D_\tau$ in $L$ and switching it in the resulting $\varphi$, we can define the "corresponding" eigenfunction $\tilde{\varphi}$ for $L^\dagger$. Writing these corresponding eigenfunctions as $\tilde{\varphi}_{n,k_x}$, the orthonormality $\langle\tilde{\varphi}_{n,k_x},\varphi_{n',k_x'}\rangle=\delta_{nn'}\delta(k_x-k_x')$ may be chosen, so long as $\langle\tilde{\varphi}_{n,k_x},\varphi_{n,k_x}\rangle\neq 0$. Shown in Appendix B, crystal structure determines linear combinations of these basis elements with respect to $k_x$; the resulting $\varphi_n$ functions are then useful for expansion purposes below. The inner product is $\langle\tilde{\varphi}_m,\varphi_n\rangle=\langle\tilde{\varphi}_m^*\varphi_n\rangle$, where the brackets $\langle\cdots\rangle$ denote an integral over space and time. Shortly we will be dealing with a periodic system and we will normalize such integrations by the unit-cell volume and the period in time. To define averages over only time or space alone, we write $\langle\cdots\rangle_\tau$ or $\langle\cdots\rangle_{\mathbf{r}}$, respectively.

### B. Solution of TDGL equation

States of the system can be parametrized by $(t,b,e,\omega)$. By changing temperature $t$, a system with some fixed $(b,e,\omega)$ may experience a normal-superconducting phase transition as temperature passes below a critical value $\tilde{t}_c(b,e,\omega)$. Such a point of transition is also known as a *bifurcation point*.

The material is said to be in the normal phase when $\Psi$ vanishes everywhere; otherwise the superconducting phase obtains, with $\Psi$ describing the vortex matter. Because of the vortices, the resistivity in the superconducting phase need not be zero. The S-N phase-transition boundary $\tilde{t}_c(b,e,\omega)$ separates the two phases. To study the condensate, we will use a bifurcation expansion to solve Eq. (5). We expand $\Psi$ in powers of distance from the phase-transition boundary $\tilde{t}_c$.

#### *1. Dynamical phase-transition surface*

As in the static case, we can locate the dynamical phase-transition boundary by means of the linearized TDGL equation.[2,14] This is because the order parameter vanishes at the phase transition and we do not need to consider the nonlinear term. The linearized TDGL equation is written as

$$L\Psi - \frac{1}{2b}(1-t)\Psi = 0. \tag{9}$$

Of the eigenvalues of $L$, only the smallest one $\varepsilon_\mathbf{0}$, corresponding to the highest superconducting temperature $\tilde{t}_c$, has physical meaning. The S-N phase transition occurs when the trajectory in parameter space intersects with the surface,

$$\varepsilon_\mathbf{0} - \frac{1}{2b}(1-t) = 0, \tag{10}$$

where the lowest eigenvalue is calculated in Appendix B,

$$\varepsilon_\mathbf{0} = \frac{1}{2} + \frac{v^2}{4(1+\omega^2)}. \tag{11}$$

Utilizing a $b$-independent frequency $\nu=b\omega$ and amplitude $e$ of input signal, we write

$$1 - t - b = \frac{e^2/2}{b^2+\nu^2}. \tag{12}$$

In the absence of external driving field, $e=0$, the phase-transition surface coincides with the well-known static-phase-transition line $1-t-b=0$ in the mean-field approach. With time-independent electric field at $\nu=0$, where the vortex lattice is driven by a fixed direction of current flow, the dynamical phase-transition surface coincides with that proposed in Ref. 10, but with a factor of 1/2. This amplitude

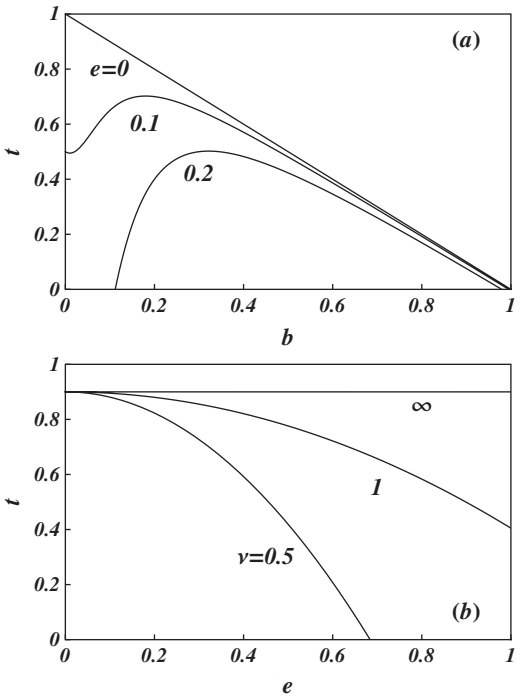


FIG. 2. Dynamical superconducting-normal phase transition. (a) Critical temperature $\tilde{t}_c$ as a function of $b$ for various $e$ at $\nu=0.1$ and (b) $\tilde{t}_c$ as a function of $e$ for various $\nu$ at $b=0.1$. The straight line in (a) is the $e=0$ curve and corresponds to the mean-field phase-transition line $1-t-b=0$. States above each line are normal phase while the region below each line is superconducting. $e$ suppresses the superconducting phase as shown in (a) while $\nu$ removes this suppression effect, as shown in (b).

difference is familiar from elementary comparisons of dc and ac circuits.

In the above equation, we can see that in the static case $e=0$, the superconducting region is $1-t-b>0$. In addition when $e\neq 0$, the superconducting region in the $b$-$t$ plane is smaller than the corresponding region in the static case, as can be seen in Fig. 2(a).

Finally, increasing frequency will increase the size of the superconducting region, as in Fig. 2(b); in the high-frequency limit, the area will reach its maximum, which is the superconducting area from the static case. As with any damped system, response is diminished at higher frequencies.

The superconducting state does not survive at small magnetic field; for example, at $e=0.2$ in Fig. 2(a), the material is in the normal state over most of the $H$-$T$ phase diagram. Later in this paper we will consider interpretation of this phenomenon. In particular, when discussing energy dissipation in Sec. III C, we will see that the main contribution to the dissipation is via the center of the vortex core. At small magnetic field, since there are fewer cores to dissipate the work done by the electric field, the superconducting state is destroyed and the order parameter vanishes.

#### 2. Perturbative expansion

That the vortex matter dominates the physical properties of the system is especially pronounced in the pinning-free flux-flow region. Here we solve Eq. (5) by a bifurcation expansion.[12,16] Since the amplitude of the solution grows when the system departs from the phase-transition surface where $\Psi=0$, we can define a distance from this surface as

$$\epsilon=\frac{1}{2b}(1-t)-\varepsilon_0 \tag{13}$$

and expand $\Psi$ in $\epsilon$. The TDGL in terms of $\epsilon$ is

$$Ł\Psi-\epsilon\Psi+\Psi|\Psi|^2=0, \tag{14}$$

where $Ł=L-\varepsilon_0$ is the operator $L$ shifted by its smallest eigenvalue. $\Psi$ is then written as

$$\Psi=\sum_{i=0}^{\infty}\epsilon^{i+1/2}\Phi^{(i)} \tag{15}$$

and it is convenient to expand $\Phi^{(i)}$ in terms of our eigenfunctions of $Ł$,

$$\Phi^{(i)}=\sum_{n=0}^{\infty}c_n^{(i)}\varphi_n. \tag{16}$$

In principle, all coefficients $c_n^{(i)}$ in Eq. (15) can be obtained by using the orthogonal properties of the basis, which are explained in Appendix B. Inserting $\Psi$ from Eq. (15) into TDGL Eq. (14), and collecting terms with the same order of $\epsilon$, we find that for $i=0$,

$$Ł\Phi^{(0)}=0 \tag{17}$$

and for $i=1$,

$$Ł\Phi^{(1)}-\Phi^{(0)}+\Phi^{(0)}|\Phi^{(0)}|^2=0. \tag{18}$$

For $i=2$,

$$Ł\Phi^{(2)}-\Phi^{(1)}+c^{(0)2}(2\Phi^{(1)}|\Phi_0|^2+\Phi^{(1)*}\Phi_0^2)=0 \tag{19}$$

and so on.

Observing Eq. (17), the solution for the equation is

$$\Phi^{(0)}=c_0^{(0)}\varphi_0, \tag{20}$$

where $\varphi_0$ is a particular linear combination of all eigenfunctions with the smallest eigenvalue.

The coefficient of $\epsilon^{1/2}$ can be obtained by calculating the inner product of $\tilde{\varphi}_0$ with Eq. (18),

$$c_0^{(0)}=\frac{1}{\sqrt{\beta_0}}. \tag{21}$$

In the same way, the coefficient of the next order $\epsilon^{3/2}$, can be obtained by finding the inner product of $\tilde{\varphi}_0$ with the $i=2$ Eq. (19),

$$c_0^{(1)}=\frac{1}{2\beta_0}\sum_{n=1}^{\infty}(2c_n^{(1)}\langle\tilde{\varphi}_0,\varphi_n|\varphi_0|^2\rangle+c_n^{(1)*}\langle\tilde{\varphi}_0,\varphi_n^*\varphi_0^2\rangle). \tag{22}$$

The inner product of $\tilde{\varphi}_m$ with Eq. (18) gives the coefficient for $m>0$,

$$c_m^{(1)} = -\frac{\beta_m/\beta_0}{\varepsilon_m - \varepsilon_0} \tag{23}$$

and

$$\beta_m \equiv \langle \tilde{\varphi}_m, \varphi_0 | \varphi_0 |^2 \rangle. \tag{24}$$

The solution of TDGL is then

$$\Psi = \epsilon^{1/2}\frac{\varphi_0}{\sqrt{\beta_0}} + \epsilon^{3/2}\sum_{n=0}^{\infty} c_n^{(1)}\varphi_n + \mathcal{O}(\epsilon^{5/2}). \tag{25}$$

In this paper we will restrict our discussion to the region near $\tilde{t}_c$ where the next-order correction can be disregarded,

$$\Psi \approx \sqrt{\frac{\epsilon}{\beta_0}}\varphi_0. \tag{26}$$

We would like to emphasize that our discussion at this order is valid in the vicinity of the phase-transition boundary and, in particular, for a superconducting system without vortex pinning. In such a system, vortices move in a viscous way, resulting in flux-flow resistivity; no divergence of conductivity is expected. Our results based on Eq. (26) were calculated at $\epsilon^{1/2}$ order, where only the lowest eigenvalue $n=0$ of the TDGL operator $L$ makes an appearance.

The next-order correction is at order $\epsilon^{3/2}$ and there is now a contribution from higher Landau levels. From the symmetry argument in Refs. 16 and 17, as long as the hexagonal lattice remains the stable configuration for the system, the next-order contribution comes from the sixth Landau level with a factor $(\varepsilon_6-\varepsilon_0)^{-1}$. Even in the putative case of a lattice deformed slightly away from a hexagonal configuration, the next contributing term is $n=2$, since in our system the lattice will remain rhombic.

### C. Vortex-lattice solution

The vortex lattice has been experimentally observed since the 1960s and its long-range correlations have been clearly observed[18] with dislocation fraction of the order $10^{-5}$. Remarkably, the same techniques can be used to study the structure and orientation of moving vortex lattice with steady current,[19] and with alternating current in the small-frequency regime.[3] In this section, we will discuss the configuration of the vortex lattice in the presence of alternating transport current in the long-time limit.

In the dynamical case, the presence of an electric field breaks the rotational symmetry of an effectively isotropic system to the discrete symmetry $y \to -y$. In contrast, a rhombic lattice preserves at least a symmetry of this kind along two axes, and the special case of a hexagonal lattice preserves sixfold symmetry.

The area of a vortex cell is determined by the quantized flux in the vortex, which is $2\pi$ in terms of our rescaled variables. As shown in Fig. 1, we choose a unit cell $C$ defined by two elementary vectors $\mathbf{a}_1$ and $\mathbf{a}_2$. We will first construct a solution for an arbitrary rhombic lattice parametrized by an apex angle $\theta_A$.

Consideration of translational symmetry in the $x$ direction leads to the discrete parameter $k_l = 2\pi l/a_1 = \sqrt{2\pi\wp}\,l$. In Appendix B we show that in the long-time limit the lowest-eigenvalue steady-state eigenfunctions of $L$ must therefore combine to form

$$\varphi_0 = \sqrt[4]{2\wp}\sum_{l=-\infty}^{\infty} e^{i(\pi/2)l(l-1)}e^{ik_l(x - v\,\sin\,\omega\tau/\omega)}u_{k_l}(y,\tau). \tag{27}$$

Here $\varphi_0$ is normalized as

$$\langle \tilde{\varphi}_0, \varphi_0 \rangle \equiv 1.$$

The function $u$ is given by

$$u_{k_l}(y,\tau) = c(\tau)e^{-(1/2)[y - k_l + i\tilde{v}\,\cos(\omega\tau - \theta)]^2} \tag{28}$$

with

$$c(\tau) = e^{-(\tilde{v}^2/4)[\sin^2\,\theta + \cos\,2(\omega\tau - \theta) + (1/2\omega)\sin\,2(\omega\tau - \theta)]}. \tag{29}$$

In analogy with a forced vibrating system in mechanics, a phase $\theta = \tan^{-1}\,\omega$ and a reduced velocity $\tilde{v} = v\,\cos\,\theta$ have been introduced for convenience in Eq. (29). The zero electric-field limit, large-frequency limit and zero-frequency limit are consistent with previous studies concluded in Appendix B.

In our approximation, the $\beta_0$ in Eq. (26) is a time-independent quantity from Eq. (24) and

$$\beta_0 = \frac{\sqrt{\wp}}{2\pi}\int_0^{2\pi} d(\omega\tau)\left\{ e^{(v_\omega^2/4)(1+\cos\,2\omega\tau + (\omega - 1/\omega)\sin\,2\omega\tau)}\sum_{p=-\infty}^{\infty} e^{-(1/2)(k_p - iv_\omega\,\cos\,\omega\tau)^2}\sum_{q=-\infty}^{\infty}(-)^{pq}e^{-(1/2)(k_q - iv_\omega\,\cos\,\omega\tau)^2)}\right\}, \tag{30}$$

where $v_\omega = v/(1+\omega^2)$.

In the small signal limit $v \to 0$, $\beta_0$ reduces to the Abrikosov constant. The Abrikosov constant with either $\theta_A = 30°$ or $60°$ minimizes the GL free energy Eq. (1) in the static state.[16] To be more explicit, $\beta_0$ can be expanded in terms of the amplitude of input signal. In powers of $v$,

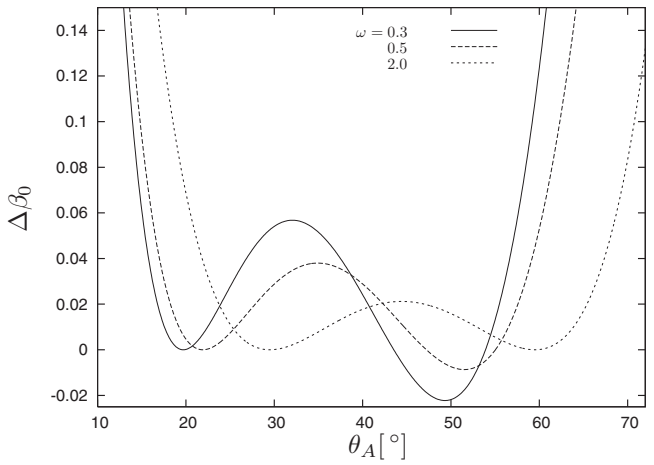


FIG. 3. Minima of $\beta_0$ can be seen for different values of $\omega$ at $v=1$.

$$\frac{\beta_0}{\beta_A} = 1 + \frac{1}{2}v_\omega^2\left(\frac{3}{2} - \frac{\beta_b}{\beta_A}\right) + \mathcal{O}(v^3) \tag{31}$$

and we find it convenient to write in terms of $v_\omega$. The first term in $\beta_0$ is the Abrikosov constant,

$$\beta_A = \sqrt{\wp}\sum_{p,q=-\infty}^{\infty}(-)^{pq}e^{-(1/2)(k_p^2+k_q^2)}. \tag{32}$$

The next term in $\beta_0$ is $v_\omega^2$ with a coefficient

$$\beta_b = \frac{\sqrt{\wp}}{2}\sum_{p,q=-\infty}^{\infty}(-)^{pq}(k_p^2+k_q^2)e^{-(1/2)(k_p^2+k_q^2)}. \tag{33}$$

We see that at high frequency, the correction in higher-order terms of $v_\omega$ can be disregarded.

For hexagonal lattices $\beta_A=2\beta_b\sim 1.159$, whereas for a square lattice $\beta_A=2\beta_b\sim 1.180$. The dependence of $\beta_0$ on $\theta_A$ can be seen in Fig. 3, where is plotted the quantity $\Delta\beta_0=\beta_0(\theta_A)-\beta_0(30°)$. For given a $\omega$ and $v$, $\beta_0$ as function of $\theta_A$ has two minima; the larger angle corresponds to the global minimum. As discussed in Eq. (31), in the high-$\omega$ limit, the two local minima become degenerate as in the static case.

## III. RESPONSE

In this section we discuss the current distribution and motion of vortices, energy transformation of the work done on the system into heat, nonlinear response, and finally the Hall effect.

### A. Motion of vortices

In addition to the conventional conductivity attributable to the normal state, there is an overwhelming contribution due to the superconducting condensate in the flux-flow regime, tempered only by the dissipative properties of the vortex matter. In this section we will examine the supercurrent density to investigate the motion of the vortex lattice. We consider a hexagonal lattice in a fully dissipative system; the nondissipative part known as the Hall effect will be discussed in Sec. III E.

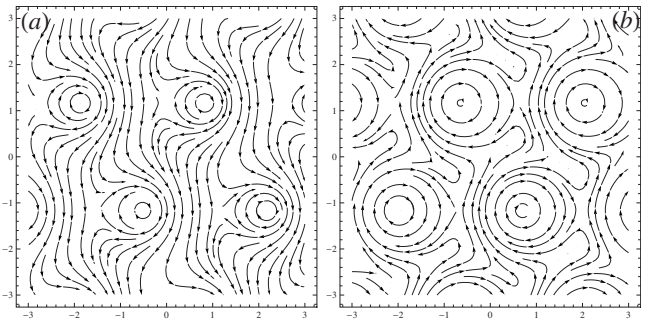


FIG. 4. Current flow at $v=1$ and $\omega=1$. (a) $t=0$; vortex cores move to the right. (b) $t=4\pi/5$; vortex cores move to the left. Vortices are drawn back and forth as the direction of the transport current density alternates. The magnitude of the current density has maximal regions which tend to circumscribe the cores; the maxima in these regions move in the plane and their manner of motion can be described as leading the motion of the vortices by a small phase. The average current in a unit cell leads the motion of the vortex in time by a phase of $\pi/2$.

The supercurrent density $\mathcal{J}(\mathbf{r},\tau)$ is obtained by substitution of the solution (26) into Eq. (4),

$$\mathcal{J}_x = \frac{\epsilon}{\beta_0}\sum_{p,q=-\infty}^{\infty}\left(\frac{k_p+k_q}{2} - y\right)g_{p,q}(\mathbf{r},\tau) \tag{34}$$

and

$$\mathcal{J}_y = \frac{\epsilon}{\beta_0}\sum_{p,q=-\infty}^{\infty}\left[\frac{i(k_p-k_q)}{2} - \tilde{v}\cos(\omega\tau-\theta)\right]g_{p,q}, \tag{35}$$

where

$$g_{p,q} = e^{-i(\pi/2)(p^2-q^2-p+q)}e^{i(k_q-k_p)[x-(v/\omega)\sin\omega\tau]}u_{k_p}^* u_{k_q}$$

and $u$ is given in Eq. (28). Observing Fig. 4, we conceptually split the current into two components. One part is the circulating current surrounding the moving vortex core as in the static case; we refer to this component as the *diamagnetic current*. The other part which we term the *transport current* is the component which forces vortices into motion. We may say that the circular current is the current which contributes to the curl of the current field with the remainder being the transport current.

The diamagnetic current may be excised from our consideration by integrating the current density over the unit cell $C$; that is, we consider $\langle\mathcal{J}\rangle_{\mathbf{r}}$. We have $\langle\mathcal{J}_x\rangle_{\mathbf{r}}=0$ and

$$\langle\mathcal{J}_y\rangle_{\mathbf{r}} = -\frac{\epsilon}{\beta_0}\tilde{v}\cos(\omega\tau-\theta)e^{-(\tilde{v}^2/4\omega)\sin 2(\omega\tau-\theta)+(v_\omega^2/2)}. \tag{36}$$

With our conventions, the transport current is along the $y$ direction. Considering the Lorentz force between the magnetic flux in the vortices and the transport current, we expect the force on the vortex lattice to be perpendicular.

We identify the locations of vortex cores to be where $|\Psi|^2=0$. The velocity of the vortex cores turns out to be

$$v_c(\tau) = \tilde{v}\cos(\omega\tau - \theta) \tag{37}$$

along the $x$ direction. Note that vortex lattice moves coherently. The vortex motion the electric field with a phase $\theta$ which increases with frequency and reaches $\pi/2$ asymptotically. The maximum velocity of vortex motion $\tilde{v}$ decreases with increasing frequency.

In Fig. 4 we show the current distribution and the resultant oscillation of vortices. As anticipated, the transport current and the motion of vortices, Eq. (37), are perpendicular as the vortices follow the input signal. The current density diminishes near the core; it is small there compared to its average value.

In steady-state motion, since the vortices move coherently in our approximation, the interaction force between vortices is balanced as in the static case. Since the system is entirely dissipative, the motion that the vortices collectively undergo is viscous flow. The vortex lattice responds to the Lorentz driving force as a damped oscillator and this is the origin of the frequency-dependent response.

### B. Configuration of moving vortex lattice

In static case the system is described by the GL equation. Solving this equation, which is Eq. (2) but with zero on the left-hand side, will select some lattice configuration. The global minima of the free energy correspond to a hexagonal lattice while there may be other configurations producing local minima. In the static case the lattice configuration can be determined in practice by building an Ansatz from the linearized GL solution[16] and then using a variational procedure to minimize the full free energy.

In the dynamic case, there is no free energy to minimize; we must embrace another method of making a physical prediction regarding the vortex lattice configuration. Let us follow Ref. 12 and take as the preferred structure the one with highest heat-generation rate. Though we have at present no precise derivation, our physical justification of this prescription is that the system driven out of equilibrium can reach steady state and stay in condensate only if the system can efficiently dissipate the work done by the driving force. Therefore, whatever the cause, the lattice structure most conducive to the maintenance of the superconducting state will correspond to the maximal heat-generation rate.

The heat-generating rate[14] is

$$\langle \dot{Q} \rangle_{\mathbf{r}} = 2\langle |D_\tau \psi|^2 \rangle_{\mathbf{r}} = \frac{\epsilon}{\beta_0}\frac{\tilde{v}^2}{2} e^{(\tilde{v}^2/2)\cos^2\theta - (\tilde{v}^2/4\omega)\sin 2(\omega\tau-\theta)} \times \left\{ \cos 2(\omega\tau - \theta) + 1 + \frac{\tilde{v}^2}{8}[\cos 4(\omega\tau - \theta) + 1] \right\}. \tag{38}$$

$\beta_0$ is given explicitly in Eq. (30) and is the only parameter involving the apex angle $\theta_A$ of the moving vortex lattice. Here $\beta_0$ plays the same role as the Abrikosov constant $\beta_A$ in the static case. Corresponding to a maximal heat-generation rate, the preferred structure can be found by minimizing $\beta_0$ with respect to $\theta_A$. That the vortex matter moves coherently is again reflected in the time independence of $\beta_0$.

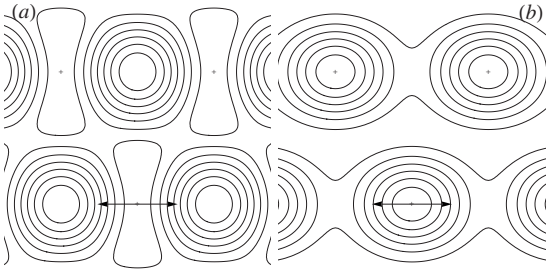


FIG. 5. Work contours of superconducting component at $v=1$ and $\omega=1$. (a) Work $\langle P \rangle_\tau$ and (b) heat-generating rate $\langle \dot{Q} \rangle_\tau$. The vortex cores are denoted by "+" in both figures, shown in the $x$-$y$ plane. The maximum displacements of vortex cores are shown by the arrow. The maximal region around the core in (a) is elongated by the current. The similar horizontal broadening around the core in (b) is caused by the vortex motion. Energy is transported; maxima in (a) and (b) do not coincide.

The minima of Eq. (30) can be seen in Fig. 3. They are such that the moving lattice is distorted away from hexagonal by the external electric field but this influence subsides at high frequency. While near the high-frequency limit there remain two local minima for $\beta_0$, the one near $\theta_A = 60°$ is favored slightly over that at 30°, as the global minimum. The two minima tend to approach each other slightly as the frequency decreases.

In an experimental setting, this provides an avenue for testing the empirical validity of the maximal heat generation prescription, in particular, in terms of the direction of lattice movement.[20] We put forth the physical interpretation that at high frequency the friction force becomes less important and the distortion is lessened. Since interactions dominate the lattice structure, the system at high frequency will have many similarities with the static case.

### C. Energy dissipation in superconducting state

Energy supplied by the applied alternating current is absorbed and dissipated by the vortex matter and the heat generation does not necessarily occur when and where the energy is first supplied. In Fig. 5, we show an example of this transportation of energy by the condensate. On the left is shown a contour plot of the work $\langle P \rangle_\tau = \langle \mathcal{J} \cdot \mathbf{v} \rangle_\tau$ done by the input signal; points along a given contour are of equal power absorption. On the right of Fig. 5 is shown the heat-generating rate,[14] $\langle \dot{Q} \rangle_\tau = 2\langle |D_\tau \psi|^2 \rangle_\tau$. The periodic maximal regions are near the vortex cores in both patterns.

In Fig. 5(b), one can see that the system dissipates energy via vortex cores. From a microscopic point of view, Cooper pairs break into quasiparticles inside the core; these couple to the crystal lattice through phonons and impurities to transfer heat. The interaction between vortices and excitation of vortex cores manifests as friction.[7]

The power loss of the system averaged over time and space is $\langle P \rangle = \langle \dot{Q} \rangle$,

$$\langle P \rangle = \frac{\epsilon}{\beta_0}\frac{\tilde{v}^2}{2} e^{(v_\omega^2/2)} \left[ I_0\left(\frac{\tilde{v}^2}{4\omega}\right) + \omega I_1\left(\frac{\tilde{v}^2}{4\omega}\right) \right], \tag{39}$$

where $I_n$ is a Bessel function of the first kind. In Fig. 6 is shown the power loss and also $\epsilon$ as a function of frequency.

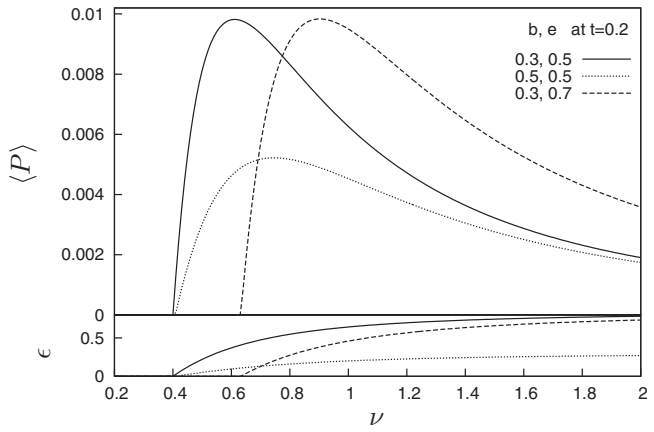


FIG. 6. Power loss of supercurrent $\langle \mathcal{J} \cdot e \rangle$ (upper panel) and expansion parameter $\epsilon$ (lower panel) as a function of frequency $\nu$.

$\epsilon$ is proportional the density of Cooper pairs and can be thought of as an indication of how robust is the superconductivity.

As frequency increases, while $\epsilon$ tends to an asymptotic value, $\langle P \rangle$ achieves a maximum and then decreases. We note that since this is a fully dissipative system the maximum in each response curve should not be considered a resonance phenomenon and cannot be associated with an effective vortex mass.

A parallel may be drawn between what we have observed in this section and the suppression of the superconductivity by macroscopic thermal fluctuations commonly observed in high-temperature superconductors. In our case, the vortices in a low-$T_c$ superconductor undergo oscillation due to the driving force of the external field. We may think of this as being analogous to the fluctuations of vortices due to thermal effects alone in a high-$T_c$ superconductor. Although the method of excitation is different, the external electromagnetic perturbation in the present case essentially plays the same role as the thermal fluctuations in high-$T_c$ situation.

Finally, we point out that $\epsilon$ seems to be an appropriate parameter for determining the amount of power loss. Generically, it seems that the power loss due to the dissipative effects of the vortex matter is diminished as the system is brought deeper inside the superconducting region of the phase diagram; that is at large $\epsilon$ compared with its saturation value at high $\nu$. We suggest the possibility that this effect, which is naïvely intuitive, is in fact physical and more widely applicable than merely the present model.

### D. Generation of higher harmonics

The practical application of superconducting materials is dependent on how well one can control the inherent nonlinear behavior. In this section we will focus on the generation of higher harmonics in the mixed state, in response to a single-frequency input signal.

The periodic transport current $\langle \mathcal{J} \rangle_{\mathbf{r}}$ is an odd function of input signal and it turns out that the response motion also contains only odd harmonics. From Eq. (36) we can calculate the Fourier expansion for transport current,

$$\langle \mathcal{J} \rangle_{\mathbf{r}} = v \ \mathrm{Re}\left[ \sum_{n=0}^{\infty} \sigma^{(2n+1)} e^{i(2n+1)\omega\tau} \right], \tag{40}$$

where the Fourier coefficient $\sigma^{(2n+1)}$ is

$$\sigma^{(2n+1)} = \frac{\epsilon e^{(1/2)v_\omega^2} i^n}{\beta_0 \sqrt{1+\omega^2}} \left[ i I_{n+1}\left(\frac{\tilde{v}^2}{4\omega}\right) + I_n\left(\frac{\tilde{v}^2}{4\omega}\right) \right] e^{-i(2n+1)\theta}. \tag{41}$$

We see the response goes beyond simple ohmic behavior and the coefficients are proportional to $\epsilon$. Experimentally, one way of measuring these coefficients is a lock-in technique[21] which is adept at extracting a signal with a known wave from even an extremely noisy environment.

To make contact with more standard parameters and satisfy our intuition, we expand the first two harmonics in terms of $v$. The fundamental harmonic, $\sigma^{(1)}$ expanded in powers of $v^2$ is

$$\sigma^{(1)} = \frac{a_h}{\beta_A(1-i\omega)} - \frac{a_h}{4\beta_A(1-i\omega)} \frac{v^2}{1+\omega^2} \times \left( \frac{1-\beta_B/\beta_A}{1+\omega^2} + \frac{1}{a_h} + \frac{i}{2\omega} \right) + \mathcal{O}(v^4), \tag{42}$$

where $a_h = (1-t-b)/2b$. The first term in Eq. (42) is the standard ohmic conductivity which we denote by $\sigma_0^{(1)}$ and is reminiscent of Drude conductivity for free charged particles. This is not an unexpected parallel since the Cooper pairs in a superconducting system can be imagined to behave like a free-particle gas. Taking this viewpoint, in the small-signal limit, the ratio $\mathrm{Im}\ \sigma/\mathrm{Re}\ \sigma = \omega = \Omega\tau_s$ gives the relaxation time of the charged particles. Subsequent higher-order corrections all contain $\omega$ in such a way that their contributions are suppressed at large $\omega$. The coefficient of the $n=1$ harmonic expanded in powers of $v^2$ is

$$\sigma^{(3)} = \frac{a_h}{8\beta_A} \frac{v^2/\omega}{\omega(3-\omega^2) - i(3\omega^2-1)} + \mathcal{O}(v^4), \tag{43}$$

which decreases quickly with increasing $\omega$.

In Fig. 7, we show the generation of higher harmonics for three different states in the dynamical phase diagram. For each harmonic labeled by $n$, $|\sigma^{(2n+1)}|$ as a function of $\nu$ has the same onset as $\epsilon$. We can see that $|\sigma^{(2n+1)}|$ reaches a maximum and then starts to decay while $\epsilon$ saturates. The coefficients of harmonics with $n>0$ decay to zero in the high-$\nu$ limit, where the state is well inside the superconducting region.

We pointed out in Sec. III C and reaffirm here that $\epsilon$ plays a significant role in determining the extent of nonlinearity in the system. In turn, the parameter which controls this is $\omega$. When $\omega$ is large, $\epsilon$ is brought closer to its saturation value $\epsilon_\infty$, causing the higher harmonics to be suppressed, and also lessening distortion of the vortex lattice. Finally, for a given harmonic, $|\sigma^{(2n+1)}|$ is generally smaller when $\varepsilon_\infty$ is smaller; this can be seen by comparing (a) and (c) of Fig. 7. One might point out that the nonlinear behavior is decreased at,

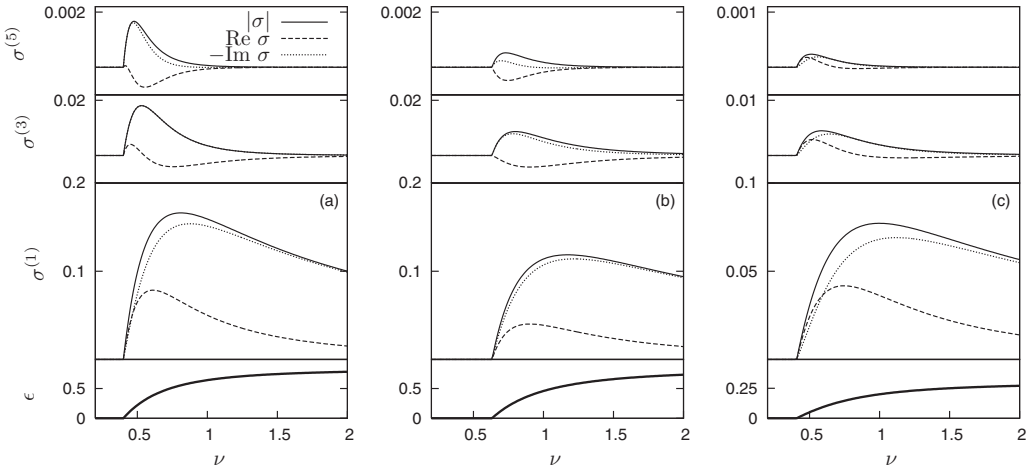


FIG. 7. Generation of harmonics: $\sigma^{(1)}$, $\sigma^{(3)}$, and $\sigma^{(5)}$ are plotted with respect to frequency $\nu$ at $t=0.2$. (a) $b=0.3$, $e=0.5$. (b) $b=0.3$, $e=0.7$. (c) $b=0.5$, $e=0.5$. The distance from the dynamic phase-transition boundary $\epsilon$ is shown in the separate bottom panel. The scale of figure (c) is half that of (a) and (b).

for example, large $\omega$. Nevertheless, we view the parameter $\epsilon/\epsilon_\infty$ as more intrinsic to the system, rather than simply characterizing the input signal.

A limited parallel can be drawn between the effect of thermal noise in high-$T_c$ superconducting systems and the effect of the electromagnetic perturbation in our present case. It seems that in either case the fluctuation influence can be reduced by adjusting the parameters to describe a state deeper inside the superconducting region of the phase diagram.

### E. Flux-flow Hall effect

In contrast to the fully dissipative system we have considered, in this section we will discuss an effect caused by the nondissipative component, namely, the Hall effect. In a clean system, vortices move without dissipation; a transverse electric field with respect to current appears. The nondissipative part is subject to a Gross-Pitaevskii description, using a type of nonlinear Schrödinger equation,[7] with a nondissipative part to the relaxation $\gamma$ from Eq. (2). The fully dissipative operator $L$ in our previous discussion can be generalized by using a complex relaxation coefficient $r=1+i\zeta$. We thus define

$$\mathcal{L} = rD_\tau - \frac{1}{2}(D_x^2 + \partial_y^2 + \partial_z^2). \tag{44}$$

The ratio $\zeta=\mathrm{Im}\ \gamma/\mathrm{Re}\ \gamma$ is typically on the order of $10^{-3}$ for a conventional superconductor and $10^{-2}$ for a high-$T_c$ superconductor.[7]

The Hall effect is small here. In normal metals, the nondissipative part gives the cyclotron frequency. If $\tau_e$ is the relaxation time of a free electron in a dirty metal, then for typical values of $\omega_c\tau_e \ll 1$ the Hall effect becomes negligible. Because the supply of conducting electrons is limited, the transverse component increases at the expense of the longitudinal component as the mean-free path of excitations grows. It is equivalent to an increase in the imaginary part of the relaxation constant at the expense of the real part.

The eigenvalues and eigenfunctions of $\mathcal{L}$ can be obtained easily by replacing the $v$ in previous results with $rv$, $\omega$ with $r\omega$ and $\tau$ with $\tau/r$. The transport current along the $x$ direction is no longer zero in the presence of the nondissipative component; it is proportional to $\zeta$. The frequency-dependent Hall conductivity can be obtained from the first-order expansion in $v$,

$$\sigma_0^{h(1)} = \frac{a_h}{\beta_A}\frac{\zeta}{(1-i\omega)^2 - \omega^2\zeta^2} \tag{45}$$

while the Hall contribution in the $y$ direction is expected to be negligible, as it is on the order of $\zeta^2$.

In principle, the crossover between nondissipative systems and dissipative systems can be tuned using the ratio $\zeta$. In a nondissipative system, which is the clean limit, the Hall effect is important and taking account of the imaginary part of TDGL is necessary. On the contrary, in a strong dissipative system where excitations are in thermal equilibrium via scattering, the purely real TDGL equation gives satisfactory agreement.

## IV. EXPERIMENTAL COMPARISON

Far-infrared spectroscopy can be performed using monochromatic radiation which is pulsed at a high rate, known as fast far-infrared spectroscopy. This technique sports the advantage of avoiding overheating in the system, making it a very effective tool in observing the dynamical response of vortices. In particular, one can study the imaginary part of conductivity contributed mainly from superconducting component.

In Fig. 8 is shown a comparison with an NbN experiment measuring the imaginary part of conductivity. The sample has the gap energy $2\Delta=5.3$ meV. The resulting value of $2\Delta/T_c$ is larger than the value expected from BCS theory.[22] We consider frequency-dependent conductivity in the case of linearly polarized incident light with a uniform magnetic field along the $z$ axis.

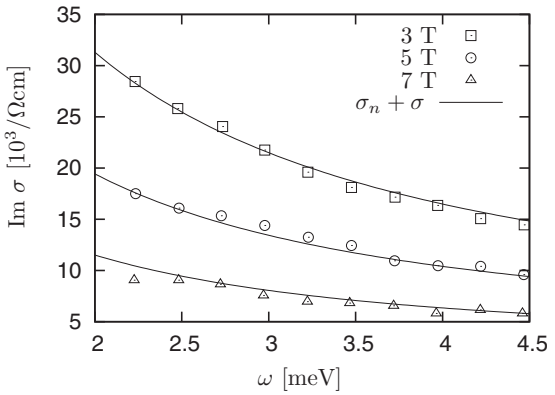


FIG. 8. Experimental comparison of imaginary part of conductivity at high frequency. The NbN experimental data are from Fig. 6(b) of Ref. 22. Material parameters $T_c^0=15.3$ K and $H_{c2}^0=14.1$ T calculated using Fig. 3(b) of Ref. 22. Normal-state conductivity is $\sigma_n=20\times10^4$ $(\mu\Omega\ \mathrm{cm})^{-1}$ and relaxation time of an electron $\tau_e=5$ fs are taken from Ref. 22. The theoretical curve has one fitting parameter $\kappa=44.5$.

The theoretical conductivity contains both a superconducting and a normal contribution. The total conductivity is obtained from the total current as in Eq. (3) where the normal-part conductivity in the condensate is the conductivity appearing in the Drude model.

According to our previous discussion, the nonlinear effect of the input signal on NbN is unimportant in the terahertz region, which corresponds to $\nu\sim17$. An approximation where the flux-flow conductivity includes only the term $\sigma_0^{(1)}$ from Eq. (42), and Hall coefficient $\sigma_0^{h(1)}$ from Eq. (45) is shown in Fig. 8 and the agreement with experiment is good.

The naive way in which we have treated the normal-part contribution is essentially inapplicable to the real-part conductivity. This is because the real-part conductivity contains information about interactions with the quasiparticles inside the core, making further consideration necessary.[23]

## V. CONCLUSION

The time-dependent Ginzburg-Landau equation has been solved analytically to study the dynamical response of the free vortex lattice. Based on the bifurcation method, which involves an expansion in the distance to the phase transition boundary, we obtained a perturbative solution to all orders. We studied the response of the vortex lattice in the flux-flow region just below the phase transition, at first order in this expansion. We have seen that there are certain parameters which can be tuned using the applied field and temperature, providing a feasible superconducting system where one can study precise control of nonlinear phenomena in vortex matter.

Under a perturbation by electromagnetic waves, the steady-state solution shows that there is a diamagnetic current circulating the vortex core, and a transport current parallel to the external electric field with a frequency-dependent phase shift and amplitude. Vortices move perpendicularly to the transport current and coherently.

Using a technique of maximizing the heat-generation rate, we showed that the preferred structure based on energy dissipation is a hexagonal lattice, with a certain level of distortion appearing as the signal is increased or the frequency is lowered. We have written transport current beyond a simple linear expression. A comparison between different harmonics of three different states in our four-dimensional parameter space indicated that the nonlinearity becomes unimportant at high frequency and small amplitude, and the response to the input signal is decreased when the system moves deeper inside the superconducting region, away from the phase-transition boundary.

To observe the configuration of moving vortices, techniques such as muon-spin rotation,[3,19] small-angle neutron scatterings,[3] scanning tunnel microscope,[24] and others[25] seem to be promising options. To provide the kind of input signal considered here, methods such as short-pulse FIR spectroscopy as used in Ref. 22 might be applied. The coefficient we defined in Eq. (41) corresponds to conductivity. We have also seen that a simple parametrization by complex quantities such as conductivity and surface impedance is insufficient to capture the detailed behavior of the system; in performing experiments, it should be kept in mind that the nonlinearity can be measured in terms of more appropriate variables as we have shown.

We have viewed the forcing of the system by the applied field to be somewhat analogous to thermal fluctuations, in the sense that they both result in vibration of the vortex lattice. Hence, the response of the vortex lattice to the electromagnetic fluctuation is stronger at the nucleation region of superconductivity than deep inside the superconducting phase. Besides, since at high frequency the motion of vortices is limited, the influence from electric field is suppressed, as is the Hall effect.

## ACKNOWLEDGMENTS

Fruitful discussions with B. Rosenstein, V. Zhuravlev, and J. Koláček are greatly appreciated. The authors kindly thank G. Bel and P. Lipavský for critical reading of the manuscript and many useful comments. The authors also have benefited from comments of A. Gurevich. F.P.-J. Lin thanks the Taiwan-Czech PPP Project for funding.

## APPENDIX A: TDGL PARAMETERS

We follow Ref. 7 to estimate the coefficient $\gamma$ which characterizes the relaxation process of the order parameter. $\gamma$ is the inverse of the diffusion coefficient for electrons in the normal state. For a strongly scattering system, as in the dirty limit,[7] the ratio between the relaxation times of order parameter

$$\tau_\Delta=\frac{\hbar^2\gamma}{2m_{ab}^*|\alpha T_c^0(1-t)|} \tag{A1}$$

and the vector potential (or current)

$$\tau_j=\frac{\beta\sigma_n 2m_{ab}^*}{8e^2|\alpha T_c^0(1-t)|} \tag{A2}$$

is

$$\frac{\tau_\Delta}{\tau_j} = \frac{\pi^4}{14\zeta(3)}. \tag{A3}$$

By definition of the thermal critical field $H_c$ and $H_{c2} = \sqrt{2}\kappa H_c$, as in Ref. 2, we know the ratio of the two parameters is

$$\frac{(\alpha T_c^0)^2}{\beta} = \frac{(H_{c2}^0)^2}{8\pi^2\kappa^2}. \tag{A4}$$

The coherence length at zero temperature can be written in terms of $H_{c2}^0$ as $\xi^2 = \Phi_0/2\pi H_{c2}^0$ and in terms of effective mass as $\xi^2 = \hbar^2/2m^*\alpha T_c^0$. As a result,

$$\gamma = \frac{2\pi^5\kappa^2\sigma_n}{7\zeta(3)c^2}. \tag{A5}$$

With $\gamma$, we can retrieve the experimental quantities from the rescaled ones used in calculation. Using the 0-subscripted original variables, we write the electric field $E = (2\hbar/e^*\xi^3\gamma)e$, and the frequency $\Omega = (2/\gamma\xi^2)\nu$. The current density $\mathbf{J}_0 = (cH^{3/2}/\sqrt{8\pi\Phi_0\kappa^2})\mathbf{J}$. In the case of linear response, we have $\mathbf{J}_0 = \sigma_0\mathbf{E}$, where $\sigma_0 = (c^2\gamma/4\pi\kappa^2)\sigma$.

## APPENDIX B: SOLVING THE LINEARIZED TDGL EQUATION

We consider the linearized time-dependent Ginzburg-Landau Eq. (9), which has been written in our chosen gauge. We wish to find the set of eigenfunctions of $L$ corresponding to the lowest eigenvalue. Based on knowledge of the solution in the static case, we solve the now time-dependent problem by making the following Ansatz.[26,27] The electric field along the $y$ direction breaks rotational symmetry in the $x$-$y$ plane, so we write

$$f(x,y,z,\tau) = e^{ik_z z}e^{ik_x x}e^{g_2(\tau)y^2 + g_1(\tau)y + g_0(\tau)}. \tag{B1}$$

After substitution of $f$ for $\Phi$ in Eq. (9), comparison of coefficients of powers of $y$ gives the following differential equations in $\tau$,

$$\dot{g}_2 + \frac{1}{2} - 2g_2^2 = 0, \tag{B2}$$

$$\dot{g}_1 + iv\cos\omega\tau - k_x - 2g_2g_1 = 0, \tag{B3}$$

$$\dot{g}_0 + \frac{1}{2}(k_x^2 + k_z^2) - \frac{1}{2}g_1^2 - g_2 = \varepsilon. \tag{B4}$$

The solutions are

$$g_2 = -\frac{1}{2}\tanh[c_2 + \tau]. \tag{B5}$$

For a steady-state solution, $\tau \to \infty$, we have $g_2 = -\frac{1}{2}$,

$$g_1 = c_2e^{-\tau} + k_x - i\tilde{v}\cos(\omega\tau - \theta). \tag{B6}$$

As with $g_1$, we have here $c_2 = 0$,

$$g_0 = -ik_x\frac{\tilde{v}}{\omega}\sin(\omega\tau - \theta) - \frac{\tilde{v}^2}{8\omega}\sin 2(\omega\tau - \theta) + c_0, \tag{B7}$$

where $c_0$ is a normalization constant.

The resulting eigenvalue is

$$\varepsilon = \frac{k_z^2}{2} + \frac{1}{2} + \frac{v^2}{4(1+\omega^2)}. \tag{B8}$$

Now, although in a more realistic treatment of the system, one may introduce some boundary condition restricting $k_z$ to a certain set of values, here we simply select the smallest eigenvalue $\varepsilon_0$ available to us by setting $k_z$ to zero. Thus equipped with the set of eigenfunctions corresponding to our lowest eigenvalue, we deem them to be the first elements of our basis, labeled by $n=0$ and $k_x$. These eigenfunctions of $L$ are

$$\varphi_{0,k_x}(x,y,z,\tau) = e^{ik_x(x - v\sin\omega\tau/\omega)}\tilde{u}_{k_x}(y,\tau) \tag{B9}$$

with

$$u_{k_x}(y,\tau) = c(\tau)e^{-(1/2)[y - k_x + i\tilde{v}\cos(\omega\tau - \theta)]^2} \tag{B10}$$

and

$$c(\tau) = e^{-(\tilde{v}^2/4)[\sin^2\theta + \cos 2(\omega\tau - \theta) + (1/2\omega)\sin 2(\omega\tau - \theta)]}. \tag{B11}$$

In the same way, the corresponding eigenfunctions of $L^\dagger$ can be obtained,

$$\tilde{\varphi}_{0,k_x}(x,y,z,\tau) = e^{ik_x(x - v\sin\omega\tau/\omega)}\tilde{u}_{k_x}(y,\tau) \tag{B12}$$

with

$$\tilde{u}_{k_x}(y,\tau) = \tilde{c}(\tau)e^{-(1/2)[y - k_x - i\tilde{v}\cos(\omega\tau + \theta)]^2}, \tag{B13}$$

where

$$\tilde{c}(\tau) = e^{-(\tilde{v}^2/4)\{\sin^2\theta + \cos 2(\omega\tau + \theta) - (1/2\omega)\sin 2(\omega\tau + \theta)\}} \tag{B14}$$

according to our normalization condition (28). The lowest eigenvalue of $L^\dagger$ is $\tilde{\varepsilon}_0 = \varepsilon_0$.

In the $\omega \to 0$ limit, the system reduces to the case of constant electric field. The eigenfunctions and eigenvalues are then consistent with those obtained by Hu and Thomson.[10] In the limit of zero electric field, the eigenfunctions and eigenvalues reduce to those of the lowest Landau-level static-state solution.[2] This is also the same in the $\omega \to \infty$ limit.

*fareh.lin@gmail.com
†pwm@induulge.net

[1] D. E. Oates, J. Supercond. Novel Magn. **20**, 3 (2007); J. C. Booth, S. A. Schima, and D. C. DeGroot, IEEE Trans. Appl. Supercond. **13**, 315 (2003); A. V. Velichko, M. Courier, J. Lancaster, and A. Porch, Supercond. Sci. Technol. **18**, R24 (2005).
[2] M. Tinkham, *Introduction to Superconductivity* (McGraw-Hill, New York, 1996).
[3] D. Charalambous, E. M. Forgan, S. Ramos, S. P. Brown, R. J. Lycett, D. H. Ucko, A. J. Drew, S. L. Lee, D. Fort, A. Amato, and U. Zimmerman, Phys. Rev. B **73**, 104514 (2006).
[4] B. Rosenstein and D. Li, Rev. Mod. Phys. **82**, 109 (2010), and references therein.
[5] A. A. Abrikosov, Zh. Eksp. Teor. Fiz. **32**, 1442 (1957).
[6] A. Gurevich and E. H. Brandt, Phys. Rev. B **55**, 12706 (1997).
[7] N. B. Kopnin, *Theory of Nonequilibrium Superconductivity* (Oxford University Press, New York, 2001).
[8] M. W. Coffey and J. R. Clem, Phys. Rev. Lett. **67**, 386 (1991).
[9] J. I. Gittleman and B. Rosenblum, Phys. Rev. Lett. **16**, 734 (1966).
[10] C.-R. Hu and R. S. Thompson, Phys. Rev. B **6**, 110 (1972); R. S. Thompson and C.-R. Hu, Phys. Rev. Lett. **27**, 1352 (1971).
[11] G. W. Crabtree, D. O. Gunter, H. G. Kaper, A. E. Koshelve, G. K. Leaf, and V. M. Vinokur, Phys. Rev. B **61**, 1446 (2000); D. Y. Vodolazov and F. M. Peeters, *ibid.* **76**, 014521 (2007).
[12] D. Li, A. M. Malkin, and B. Rosenstein, Phys. Rev. B **70**, 214529 (2004).
[13] B. Rosenstein and V. Zhuravlev, Phys. Rev. B **76**, 014507 (2007).
[14] J. B. Ketterson and S. N. Song, *Superconductivity* (Cambridge University Press, Cambridge, 1999).
[15] L. L. Gor'kov and G. M. Eliashberg, Zh. Eksp. Teor. Fiz. **54**, 612 (1968); A. Schmid, Phys. Kondens. Mater. **5**, 302 (1966).
[16] G. Lasher, Phys. Rev. **140**, A523 (1965).
[17] D. Li and B. Rosenstein, Phys. Rev. B **60**, 9704 (1999).
[18] P. Kim, Z. Yao, C. A. Bolle, and C. M. Lieber, Phys. Rev. B **60**, R12589 (1999).
[19] D. Charalambous, P. G. Kealey, E. M. Forgan, T. M. Riseman, M. W. Long, C. Goupil, R. Khasanov, D. Fort, P. J. C. King, S. L. Lee, and F. Ogrin, Phys. Rev. B **66**, 054506 (2002).
[20] A. T. Fiory, Phys. Rev. Lett. **27**, 501 (1971).
[21] M. O. Sonnaillon and F. J. Bonetto, Rev. Sci. Instrum. **76**, 024703 (2005).
[22] Y. Ikebe, R. Shimano, M. Ikeda, T. Fukumura, and M. Kawasaki, Phys. Rev. B **79**, 174525 (2009).
[23] P.-J. Lin and P. Lipavský, Phys. Rev. B **80**, 212506 (2009).
[24] A. M. Troyanovski, J. Aarts, and P. H. Kes, Nature (London) **399**, 665 (1999).
[25] T. H. Johansen, http://www.fys.uio.no/super/vortex
[26] C. F. Lo, Phys. Rev. A **47**, 115 (1993).
[27] B. Rosenstein (private communication).